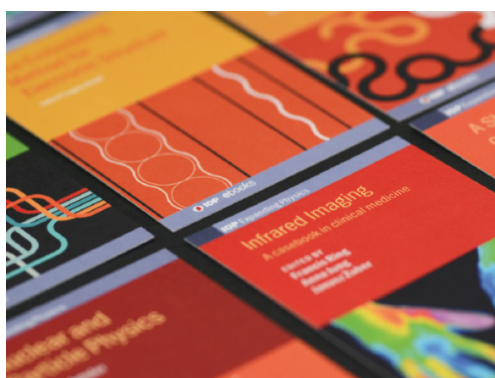**PAPER • OPEN ACCESS**

Surface optical reflectance combined with x-ray techniques during gas-surface interactions

To cite this article: S Albertin *et al* 2020 *J. Phys. D: Appl. Phys.* **53** 224001

View the article online for updates and enhancements.

Recent citations

- Recent advances in surface x-ray diffraction and the potential for determining structure-sensitivity relations in single-crystal electrocatalysis
Gary S. Harlow *et al*

Surface optical reflectance combined with x-ray techniques during gas-surface interactions

S Albertin[1], J Gustafson[1], J Zhou[2], S Pfaff[2] , M Shipilin[3], S Blomberg[4], L R Merte[5], O Gutowski[6], A-C Dippel[6], J Zetterberg[2], E Lundgren[1] and U Hejral[1]

[1] Division of Synchrotron Radiation Research, Lund University, Box 118, S-221 00, Sweden
[2] Division of Combustion Physics, Lund University, SE-22100 Lund, Sweden
[3] Division of Chemical Physics, Stockholm University, SE-10691 Stockholm, Sweden
[4] Department of Chemical Engineering, Lund University, SE-22100 Lund, Sweden
[5] Materials Science and Applied Mathematics, Malmö University, 204 06 Malmö, Sweden
[6] Deutsches Elektronen-Synchrotron DESY, D-22607 Hamburg, Germany

E-mail: Stefano.Albertin@sljus.lu.se and Uta.Hejral@sljus.lu.se

Abstract

High energy surface x-ray diffraction (HESXRD), x-ray reflectivity (XRR), mass spectrometry (MS) and surface optical reflectance (SOR) have been combined to simultaneously obtain sub-second information on the surface structure and morphology from a Pd(100) model catalyst during *in situ* oxidation at elevated temperatures and pressures resulting in Pd bulk oxide formation. The results show a strong correlation between the HESXRD and SOR signal intensities during the experiment, enabling phase determination and a time-resolved thickness estimation of the oxide by HESXRD, complemented by XRR measurements. The experiments show a remarkable sensitivity of the SOR to changes in the surface phase and morphology, in particular to the initial stages of oxidation/reduction. The data imply that SOR can detect the formation of an ultrathin PdO surface oxide layer of only 2–3 Å thickness.

Supplementary material for this article is available online

(Some figures may appear in colour only in the online journal)

1. Introduction

Surface science is of tremendous importance for a large number of fundamental and applied fields such as nano-technology, electrochemistry, medical technology, semiconductor technology, and catalysis [1]. Especially, heterogeneous catalysis, is and has been, a major motivation for surface studies of single crystal model catalysts [2]. For decades, the adsorption, desorption and chemical reactions at relevant surfaces have been studied in ultra-clean, well-controlled, ultra high vacuum (UHV) conditions, providing a detailed understanding of gas–surface interactions. However, in recent years there has been an effort to investigate more complex and more realistic model catalysts and reaction environments, in an effort to bridge the so-called pressure and materials gaps between fundamental surface science studies and industrial catalysts. As a consequence, a wide range of techniques have been developed in an effort to probe surface structures during a catalytic reaction at elevated pressures and temperatures. For many years, polarization modulation-infrared reflection absorption spectroscopy (PM-IRAS) [3, 4], x-ray absorption spectroscopy (XAS) [5] and sum frequency generation (SFG) [6] were

J. Phys. D: Appl. Phys. **53** (2020) 224001

S Albertin *et al*

the state-of-the art techniques that allowed for *in situ* studies of well-defined surfaces. Recent experimental advances have resulted in ambient pressure x-ray photoelectron spectroscopy (APXPS) [7–9], high-pressure scanning tunneling microscopy (HP-STM) [10], *in situ* surface x-ray diffraction (SXRD) [11] and environmental transmission electron microscopy (E-TEM) [12], resulting in an extension of the *in situ* experimental toolbox.

Through this effort, it has been understood that some oxide structures on the Pt group metals are active phases in CO oxidation, and that the activity depends on the exact arrangement of the surface atoms and the availability of coordinatively unsaturated sites (CUS). For instance, the surface oxides on Ru(0001) and Pd(100) are active in CO oxidation due to the undercoordinated Ru atoms in the $RuO_2(110)$ and Pd atoms in the PdO(101) surfaces [13, 14], while the surface oxide on Rh surfaces is not active [15, 16], since the oxide is oxygen terminated. Interestingly, there is a continued discussion, and to some extent, a disagreement between UHV and semi-realistic investigations on the relative activity between various phases [16, 17]. It is therefore well-motivated to develop new experimental techniques for a better understanding of the atomistic processes governing a catalytic reaction both in UHV and under semi-realistic conditions.

Surface optical reflectance (SOR) has traditionally been used to study pitting corrosion [18, 19], but has recently also shown to be a promising *in situ* and *operando* technique during catalytic reactions [20–23]. Given its simplicity, low cost, *in situ* and *operando* compatibility, and the fact that it can readily be installed at various experimental setups to give complementary information, SOR is a very attractive technique. The change in the reflected intensity observed in the SOR measurements, however, is partly due to a change in roughness and partly due to a change in the optical properties such as refraction and damping/absorption. In the present case, as the Pd(100) metal surface oxidizes forming PdO, the surface roughens and the optical properties change simultaneously, making the two effects difficult to disentangle.

To this end, we have performed simultaneous measurements of high energy surface x-ray diffraction (HESXRD), x-ray reflectivity (XRR), mass spectrometry (MS) and SOR, to correlate the surface structural changes, monitored by means of HESXRD, to the changes in the SOR signal during the oxidation of Pd(100). We find that the SOR is remarkably sensitive to subtle changes in surface morphology such as an increasing/decreasing surface roughness and/or the oxidation of the material, already at an initial oxidation featuring the formation of an ultrathin 2D Pd surface oxide only. At a later oxidation state, we correlated the thickness of a growing Pd oxide film, as determined by HESXRD and XRR, to changes in SOR signal intensity. The data showed temporal discrepancies between changes monitored in the SOR and changes in the intensities of bulk oxide Bragg peaks measured by HESXRD, especially in the onset of the sample oxidation and reduction. These discrepancies, along with the potential use of SOR and its combination with x-ray techniques, will be discussed.
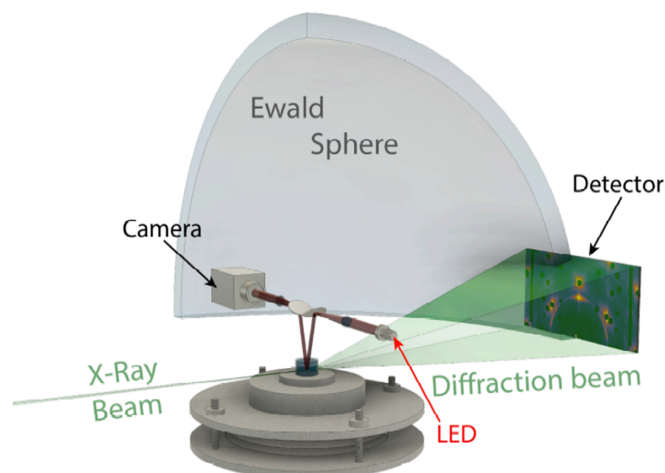

Figure 1. Schematics of the experimental setup at beamline P07 at PETRA III, DESY. In light green: incoming and diffracted x-ray beams. The diffracted x-rays are recorded on a large 2D detector centred around the reciprocal space origin (000). The bottom center of the image displays the in-situ catalysis chamber [25] equipped with a sapphire dome for optimal x-ray and optical access. The optical system consists of a 4*f* setup with red LED as source, camera and associated optics for data collection [22, 23].

2. Experimental

The experiment was performed in experimental hutch 2 (EH2) of the high energy materials science beamline P07 at Petra III, Deutsches Elekronen-Synchrotron (DESY) in Hamburg, Germany [24]. As sample environment a dedicated *in situ* catalysis chamber [25] that allows both, UHV preparation of the sample surface as well as operando catalysis studies in a reactor cell, was used. The reactor cell provides a computer-controlled introduction of gases, where the gas composition inside the cell is constantly being probed by leaking into a mass spectrometer. In the present experiment, the gases O_2, diluted CO (10% CO in 90% Ar) as well as pure Ar (carrier gas) were used. The SOR setup was mounted onto the catalysis chamber top plate. To allow for simultaneous x-ray (HESXRD and XRR) and optical access (SOR) to the sample surface, the high pressure reactor part of the chamber was enclosed by a sapphire dome [23, 26]. A schematic drawing of the experimental setup is shown in figure 1.

As sample a hat-shaped and round Pd(100) single crystal was used, where the polished surface area featured a diameter of 6 mm. To describe the crystal structure, a tetragonal set of vectors was used, with $\mathbf{a}_1$ and $\mathbf{a}_2$ defining the surface plane and $\mathbf{a}_3$ the out-of-plane direction. The lengths of these vectors can be expressed as $|\mathbf{a}_1| = |\mathbf{a}_2| = \frac{a_0}{\sqrt{2}}$ and $|\mathbf{a}_3| = a_0$, with $a_0 = 3.89$ Å refering to the bulk lattice constant of Pd. A ball model of the investigated PdO(101) bulk oxide on top of the Pd(100) surface using the unit cell parameters discussed in [27] is shown in figure 2. The PdO(101) surface is of great interest in catalysis studies as it contains coordinatively unsaturated sites (cus) that may act as active centers [28].
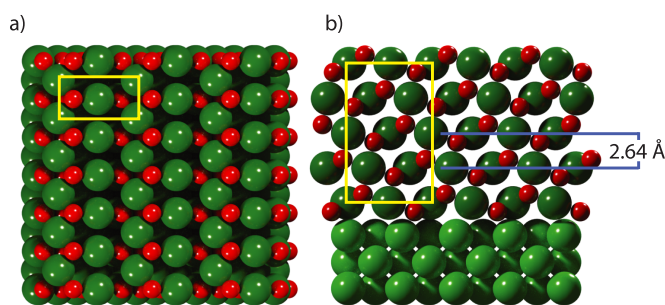
a)   b)

Figure 2. (a) Top and (b) side view of the PdO(101) bulk oxide with the unit cell highlighted by a yellow square and the interlayer distance of 2.63 Å marked by dark-blue horizontal lines.

For the x-ray measurements the photon energy was set to 77 keV, with a photon flux of approximately 5×10^{10} photons per second. An incident angle of the x-ray beam of $0.05°$, close to the critical angle of Pd, enhanced the diffracted signals from the sample surface compared to diffraction signals from the bulk. For the HESXRD measurements, a PerkinElmer flat panel x-ray detector, especially suited for x-ray photon energies higher than 20 keV, was used (410×410 mm^2 total size, 200×200 μm pixel size and total resolution of 4 MP). Due to high intensity x-ray reflections above the detector saturation level from Bragg peaks of the sapphire dome and the bulk Pd, tungsten beam-stops were put in front of the detector to block the corresponding signals to avoid detector damage. These beam-stops consequently left corresponding circular shadows in the detector images, as can be seen in figures 3(a), (b) and (e).

The SOR setup consisted of a 700 mW LED (Thorlabs M625L3) with a wavelength of 650 nm as well as of a 2D sCMOS camera (Andor Zyla) with 2048×2048 pixel resolution (pixel size: 6.5 μm) and a maximum acquisition rate of 200 Hz [22, 23]. In the present experiment, an acquisition rate of 10 Hz was used. To suppress intensity irregularities of the internal LED pattern, a spatial filter was used to diffuse the LED light just after the source. Thereafter, the LED light was collimated before directing it onto the sample surface from above, which was done by using a mirror placed at a $10°$ angle. Using a second mirror at the same angle, the reflected beam was caught and directed onto the camera using a $4f$-setup. Since the LED equipment was mounted on top of the catalysis chamber, the chamber movements during the HESXRD measurements caused vibrations. Accordingly, 'wave-like' artifacts across the sample surface are visible in the SOR images after image subtraction, as can be deduced from figures 3(c) and (d). Moreover, imperfections in the sapphire dome material resulted in two round artifacts of reduced reflected intensity.

To complement our HESXRD data and to obtain information on the respective oxide layer thickness as well as the surface and interface roughnesses, x-ray reflectivity measurements (XRR) were performed using a NaI scintillation point detector. The data was analysed using the GenX 2.4.10 software [29].

Prior to the *in situ* oxidation measurements, the sample surface was prepared using the UHV part of the catalysis chamber. The surface preparation consisted of cycles of Ar$^+$ sputtering (20 min at $U_{acc} = 1.5$ keV, $p_{Ar} = 5 \times 10^{-5}$ mbar) and annealing at ~950 $°$C for 5 min without exposing the sample to any gases in the low 10^{-7} mbar range. In addition, the Pd(100) sample was just before the oxidation experiment exposed for several minutes to a reducing gas mixture consisting of a CO flow of 16 ml min^{-1} and an Ar flow of 144 ml min^{-1} at 370 mbar total pressure and 300 $°$C, to ensure a metallic surface. The diffraction pattern shown in figure 3(a) was measured under these conditions. It contains sharp crystal truncation rod signals of high intensity, characteristic of a smooth and metallic Pd(100) surface [30, 32].

3. Results

The experiment reported here consisted of the oxidation of the sample under the flow of an O$_2$/Ar mixture and its subsequent reduction using a CO/Ar mixture. Previously, we have in detail investigated the surface structures evolving during CO oxidation over a Pd(100) surface using HESXRD [30–33]. We showed that as the oxygen excess in the O$_2$:CO ratio is increasing, the surface structures develops from a clean Pd(100) to a $(\sqrt{5} \times \sqrt{5})$R27$°$ surface oxide, followed by the growth of epitaxial PdO(101) bulk oxide islands on top of the surface oxide, and finally by the growth of a thicker and more powder like poly-crystalline PdO [31]. This epitaxial and Stransky-Krastanov growth of the PdO(101) on Pd(100) was also recently confirmed using atomic oxygen from a plasma source with low energy electron diffraction (LEED) and temperature programmed desorption (TPD) [17]. In the following it will be described how time-resolved HESXRD measurements can be correlated to changes detected by means of SOR during oxide formation on Pd(100).

The timeline of the *in situ* oxidation experiment is summarized in figure 4, where its bottom part contains the partial pressures of O$_2$, CO and Ar as measured by means of MS during the different probed conditions. In the following all given points in time *t* will correspond to changes made in the gas settings (gas flow settings of the mass flow controllers). Due to the distance between the reactor mass flow controllers and the mass spectrometer situated at the chamber, a delay of around 7 s is observed in the MS data. Accordingly, at around t = 49 s the gas flows were changed from reducing conditions containing CO gas (condition 1: 16 ml/min CO, 144 ml/min Ar, p$_{tot}$ = 370 mbar) to pure Ar flow (condition 2: 160 ml/min Ar, p$_{tot}$ = 370 mbar). Thereafter, at around t = 168 s, O$_2$ was introduced (condition 3: 16 ml/min O$_2$, 144 ml/min Ar, p$_{tot}$ = 370 mbar). After this *in situ* oxidation, the gas flows were first switched back to pure Ar flow at t = 1820 s (condition 2), before the sample was reduced by CO introduced at t = 1898 s (condition 1). Throughout the experiment, the sample temperature was kept constant at 300 $°$C.

Throughout the time-span of the oxidation (t = 0 s→t = 1820 s) and the reduction (1898 s→2000 s), both SOR and HESXRD images were continuously acquired.
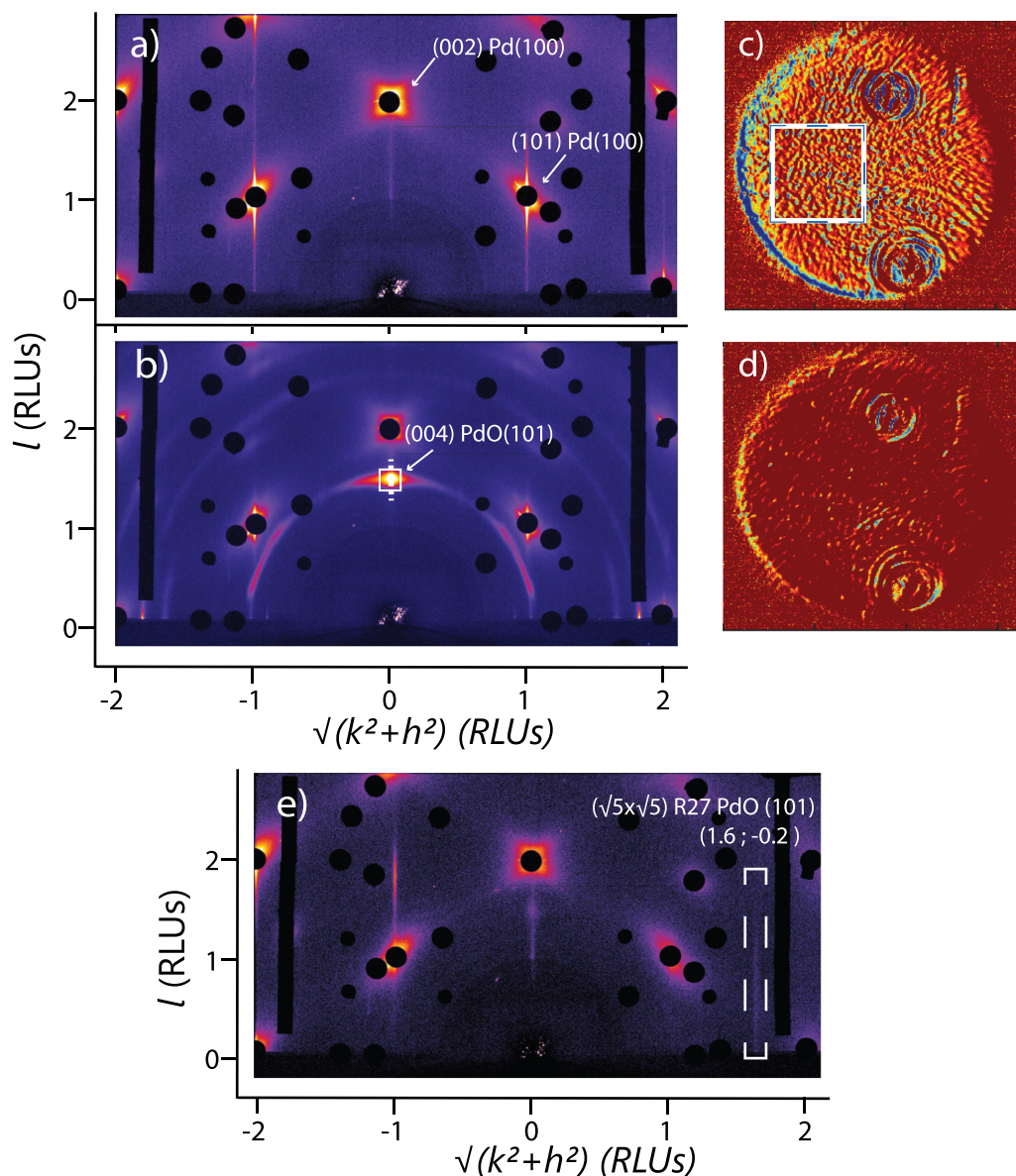
Figure 3. Integrated diffraction patterns over a full rotation (a) before oxidation (clean sample) and (b) after oxidation. The white square in (b) indicates the region of interest used for integrating the diffracted intensities of the (004) PdO(101) Bragg peak. The white dashed line in (b) denotes the position for the linescans extracted in *l*-direction used for fitting the Bragg peaks to obtain information on the PdO(101) bulk oxide height. The tungsten beam stoppers that protect the detector from the bulk reflections from Pd and sapphire are seen as black, round objects. (c) SOR image before oxidation, (d) SOR image after oxidation. The white square indicates the region of interest used for integrating the reflected intensities. The SOR images contain two areas of reduced reflected intensity caused by imperfections in the sapphire dome as well as wave-like patterns caused by the diffractometer movements. (e) Single HESXRD image taken at t = 220 s and extracted from a rotational scan, showing rod signals from the Pd $(\sqrt{5} \times \sqrt{5})$R27° surface oxide and a faint signal of the (004) PdO(101) Bragg peak.

In the case of the HESXRD measurements, 2D reciprocal space maps were taken while the catalysis chamber including the sample were continuously rotated back and forth to completely include the $(\pm 1,0,l)$ Pd Crystal Truncation Rod (CTR), thereby covering a total angular space of 15°. The total time for a full 15° rotation comprised 10.5 seconds, during which 16 images were taken, resulting in an exposure time of 0.65 s per image. Figures 3(a) and (b) show 2D diffraction patterns obtained by the integration of such rocking scans, in which the highest intensity value for each pixel position after comparison of all images of the entire data set of one rotation

was taken, thus projecting the total angular space of 15° onto a 2D image.

Figure 3(a) displays the HESXRD 2D projection measured before *in situ* oxidation, figure 3(b) displays it after, where the corresponding timestamps of when the scans were measured are indicated by a and b in figure 4, respectively. The 2D projection of figure 3(a) shows distinct crystal truncation rod signals of high intensity, running through the bulk Pd Bragg peaks. They indicate the presence of a clean and smooth Pd(100) surface prior to the *in situ* oxidation. Contrary, in the HESXRD 2D projection obtained after oxidation displayed
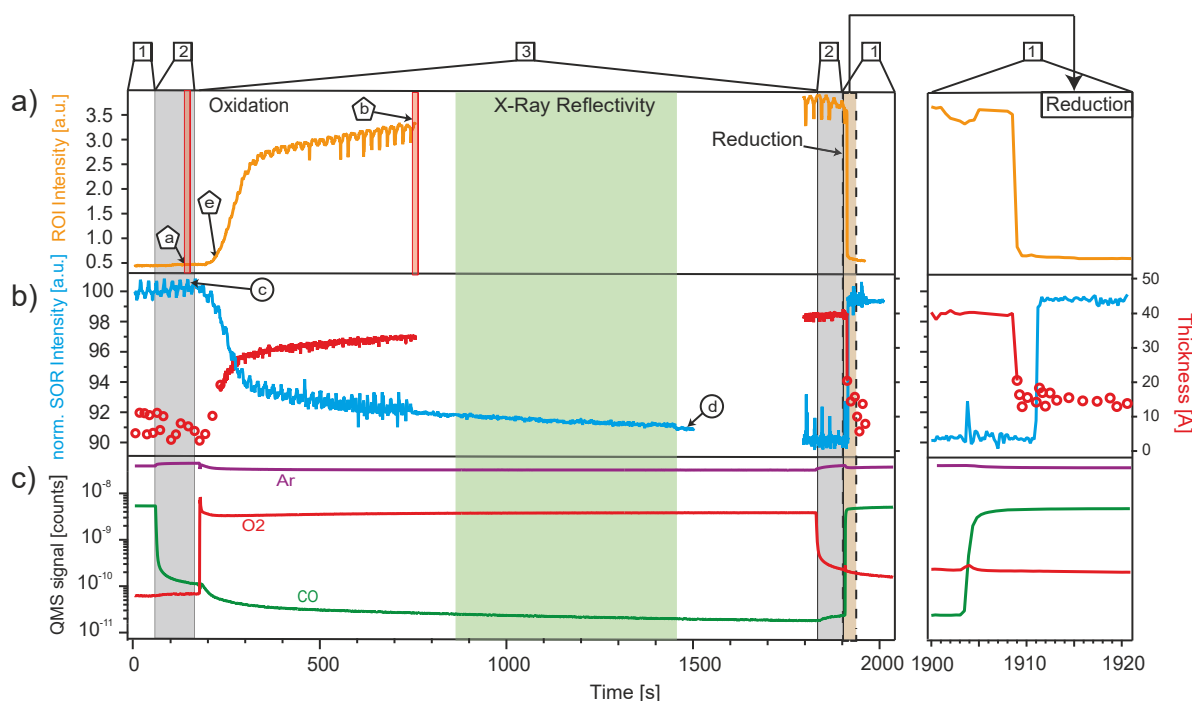
Figure 4. Direct comparison of HESXRD, SOR and MS data as function of time during oxidation and reduction, where the numbers '1', '2' and '3' refer to periods of different gas flows/composition (see text for more detail). The left panels show the entire experiment while the panels on the right correspond to close-ups on the dashed areas of the reduction process. The light-green box corresponds to the time interval of the XRR measurements. (a) Region of interest (ROI) intensity: intensity of the (004) PdO(101) Bragg peak signal of the HESXRD images integrated over the area indicated by the white square in figure 3(d). 'a', 'b', 'e' denote the respective points in time when the HESXRD images displayed in figures 3(a), (b) and (e) were measured. (b) Blue line: integrated SOR intensities, where 'c' and 'd' indicate the respective points in time when the SOR images displayed in figures 3(c) and (d) were measured. Red line/red open circles: thickness of the PdO(101) bulk oxide as deduced from fits to linescans extracted in vertical direction through the (004) PdO(101) Bragg peak (red line: confidence of fit higher than 2σ, red circles: confidence of fit below 2σ). (c) Partial CO, O_2 and Ar pressures as measured by MS. More information on the onset of oxidation can be found in the supplementary information.

in figure 3(b) the intensity of the crystal truncation rods are greatly reduced, indicating a roughening of the Pd(100) surface. In addition, new diffraction features appeared during the oxidation. Thus, Bragg peaks at reciprocal space positions in line with the formation of epitaxial bulk PdO(101) appeared, as well as ring-like features. The latter point towards the formation of polycrystalline PdO, in agreement with the results found for a highly oxidized Pd(100) surface [31].

The HESXRD results just discussed are in well agreement with our SOR measurements. Figures 3(c) and (d) show SOR images taken before and after the oxidation, respectively, corresponding to the timestamps indicated by c and d in figure 4. They show the top view of the reflected intensity from the full round sample surface (diameter: 6 mm). In line with the HESXRD results, the SOR image measured before oxidation shown in figure 3(c) reveals a high level of reflected intensity over the whole sample surface, in line with the notion of having a metallic and smooth Pd(100) surface prior to oxidation. Contrary, the SOR image measured after oxidation in figure 3(d) reveals a highly reduced reflected intensity, indicating 1) a roughening of the total surface area as can be caused by the formation of PdO(101) oxide islands as witnessed in the HESXRD, and/or 2) a change in the optical parameters of the sample surface, which can also be traced back to oxide formation.

In order to evaluate the sensitivity of the SOR technique, the temporal evolution of the SOR intensity was compared to the intensity evolution of selected HESXRD diffraction signals during the oxidation and reduction process, which is summarized in figure 4. The intensity integrated over the area indicated by the white square in the SOR data of figure 3(c) plotted as function of time is displayed as blue line in figure 4(b), while the intensity integrated over the (004) Bragg peak of the PdO(101) bulk oxide, indicated by the white square in figure 3(d), is displayed as orange line ('ROI Intensity', ROI = 'region of interest') in figure 4(a). The periodic wiggles in the intensities of the SOR data and the (004) Bragg peak intensity are due to the vibrations caused by the in-situ catalysis chamber continuously rotating back and forth during the experiment, and have a periodicity of 10.5 s, the duration of a full rotation of the setup.

When exposing the metallic Pd(100) surface to O_2 at t = 168 s, an increase in O_2 partial pressure was detected by the mass spectrometer (figure 4(c)). Shortly after this, the SOR signal intensity started to decrease, featuring a more rapid decrease for t $\leq$ 310 s, while the rate of the decrease slowed down significantly for t $\geq$ 310 (figure 4(b)). The more distinct onset of the decrease in the SOR signal at around t = 200 s correlates with the appearance of the Pd ($\sqrt{5} \times \sqrt{5}$)R27° surface oxide, diffraction signals of which were detectable in the

time interval of t = 203 s → t = 277 s. Figure 3(e) shows a diffraction image containing superstructure rod signals from the surface oxide. The presence of this ultrathin 2D oxide layer coinciding with a decrease in the SOR signal indicates that SOR can detect this only 2–3 thin surface oxide layer.

Only at t = 210 s, with a delay of about 42 s after the introduction of O_2 (t = 168 s), we monitored the appearance of first traces of the (004) Bragg peak of the PdO(101) bulk oxide, as well as a gradual increase in its intensity (figure 4(a)), indicating the formation and the gradual growth of crystalline and epitaxial PdO(101) bulk oxide islands. The 2D image of figure 3(e) mentioned earlier and taken at t = 220 s reveals not only a fingerprint diffraction signal of the surface oxide. It also contains already signal intensity of the (004) PdO(101) Bragg peak since at this point in time the surface oxide was coexisting with the bulk oxide. Comparable to the trend of the SOR intensity the rate of the (004) Bragg peak intensity change was very high at the beginning, and slowed down significantly at around t = 310 s. This trend indicates that the oxide growth was faster at the beginning and slowed down at around t = 310 s. This finding is in line with a self-limited bulk oxide growth in which the diffusion of the metal and oxygen ions, that build up the oxide layer, is driven by the electric field between them [34–37]. This field becomes weaker above a certain critical oxide layer thickness, and the rate of oxide growth is accordingly significantly slowed down. More information on the onset of oxidation is shown in figure S1 in the supplementary information (stacks.iop.org/JPhysD/53/224001/mmedia).

To obtain quantitative information on the time-resolved bulk oxide growth, linescan profiles were extracted along *l*-direction through the (004) PdO(101) Bragg peak. The area used for extracting the linescans is indicated by the dashed white line in figure 3(b). Fitting these profiles with Gaussian functions provided full widths at half maximum from which the respective oxide heights as a function of time were calculated. The thus deduced oxide heights are represented by the solid red line and the red circles in figure 4(b). The fit results are presented only if the confidence of the fit, $\frac{\Delta E}{E}$, was above the standard deviation 2σ. This was the case for all images after t≥220 s, where the fit results are represented by the solid line. For t≤220 s it was not possible to retrieve fittings with the desired confidence, but to illustrate a general trend for t≤220 s, the fit results for t≤220 s are represented by red circles.

The data shows that during the time interval between t = 168 s, when O_2 was introduced, and t = 310 s, the oxide thickness was rapidly increasing from 0 to 25 Å within 142 s. Thereafter, the speed of the growth was slowing down, in line with the aforementioned notion of a self-limiting oxide growth. At t = 600 s, the HESXRD measurements were interrupted in order to perform x-ray reflectivity measurements. At approximately t = 1800 s, about 27 min after the introduction of O_2, the HESXRD measurements were restarted, revealing an ultimate PdO(101) thickness of almost 40 Å.

The x-ray reflectivity measurements on the oxidized Pd(100) sample were probed between t = 850 s and t = 1450 s and complemented the HESXRD and SOR data. The experimental data is represented as open circles in figure 5(a), the
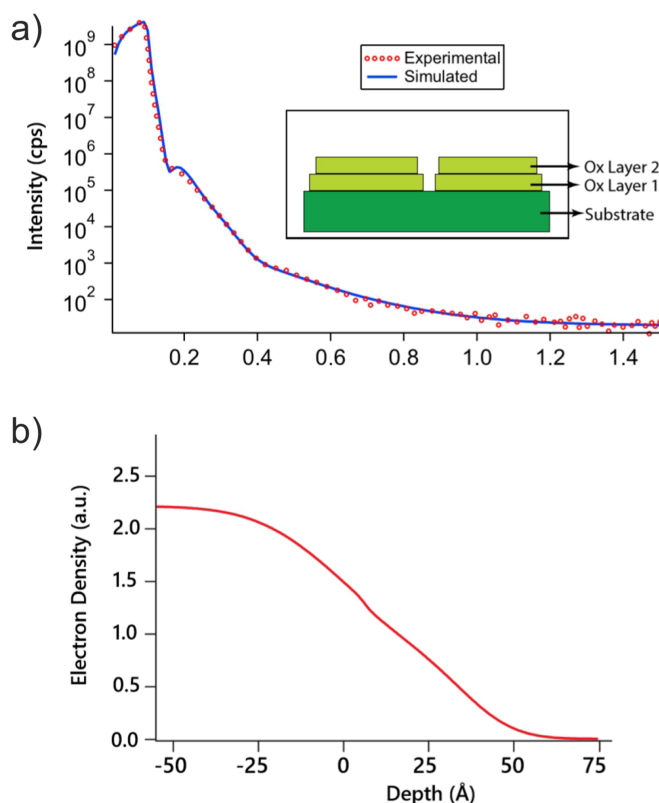

Figure 5. XRR results after oxidation of the Pd(100). (a) Red circles represent the experimental data, the blue line represents the fit to the data. Inset: Two-box model used as underlying fit model, light green: oxide islands, dark green: Pd(100) substrate. (b) Electron density profile obtained from the fit plotted as function of distance from the Pd(100) sample surface

fit to the data is shown as solid line. As underlying fit model, a two-layer box model for the PdO(101) oxide on top of the Pd(100) substrate was used (see inset of figure 5(a)). The fit parameters included the heights (h_1, h_2), the electron densities (ρ_1, ρ_2) and the surface roughnesses (σ_1, σ_2) of the individual layers, as well as the interface roughness to the Pd(100) substrate (σ_{sub}). For each layer the surface and interface roughness σ_x is treated as Gaussian-shaped fluctuations around an average layer thickness h_x, with σ_x describing the root mean square of the corresponding height deviations from h_x. The electron density profile obtained from the fit is shown in figure 5(b). The thus deduced total thickness of the oxide ($h_{tot} = h_1+h_2$) amounts to 36.3 Å, in good agreement with the expected value from the HESXRD measurements. The overall shape of the two-layer model, with a much thinner bottom oxide layer ($h_1 = 6.3$ Å) covering 46% of the sample surface, and a thicker upper layer ($h_2 = 30.0$ Å) covering 43% of the sample surface with a toplayer roughness of $\sigma_1 = 12$ Å, results in a smeared out profile of the PdO bulk oxide electron density. It is shown in figure 5(b) and is in good agreement with previous measurements reporting a Stranski-Krastanov growth mode [17, 32].

After the *in situ* oxidation experiment, the O_2 flow was switched off and the sample was exposed to pure Ar flow at t = 1818 s (condition 2). At t = 1897 s, CO was introduced again (condition 1), resulting in a reduction and complete restoration of the Pd(100) surface since the PdO(101) signals
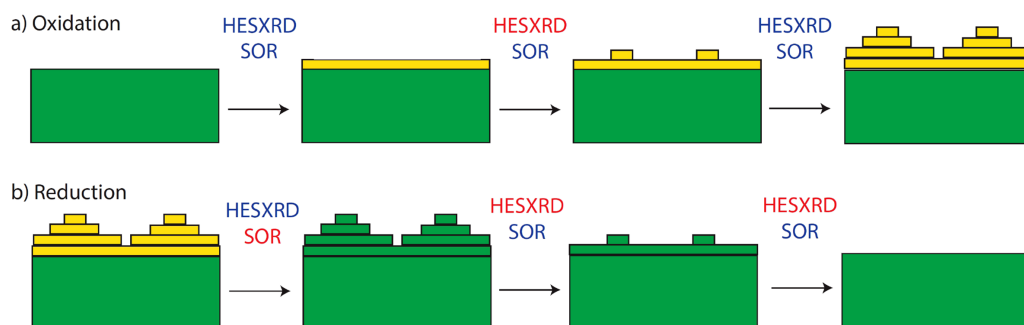
Figure 6. Schematics illustrating the oxidation and reduction processes in which green is Pd and yellow PdO. Blue (red) text indicates a detectable (non-detectable) change. (a) The oxidation process. (b) The reduction process.

completely disappeared and the Pd CTRs in the HESXRD pattern appeared again (see figure S1 in the supplementary information). Moreoever, with a delay of about 3 s after the dirsappearance of the oxide diffraction peaks in the HESXRD data, the sudden and complete recovery of the SOR signal to the same high level of the metallic surface was evidenced.

4. Discussion

It is interesting to note that during the oxidation process, HESXRD monitored the bulk oxide (004) Bragg peak 42 s, and the Pd surface oxide 37 s after the introduction of O_2. Contrary, the first signal change in the SOR was detected already 20 s after the introduction of O_2 (see figure S1 in the supplementary information). On the other hand, the HESXRD detects the reduction of the bulk oxide approximately 3 s prior to the SOR. It should be emphasized that the reasons for these observations are not clear, however we may speculate, and they will accordingly be discussed below.

A possible scenario is shown in figure 6, in which simplified models of the oxidation and reduction processes can be seen. During the first stages of the oxidation, an initial wetting layer of PdO surface oxide is detected by both, the SOR, which detects an immediate decrease in signal intensity, and the HESXRD, monitoring surface oxide rods. Shortly thereafter, small islands of PdO bulk oxide are formed in addition [10, 38]. These are only detected by the SOR, leading to a continous decrease in the SOR signal due to increasing roughening. These PdO bulk oxide islands are, however, not monitored by HESXRD, since the PdO domains are initially too small to render Bragg peak signals distinguishable from the general HESXRD detector background. In the present case, an oxide thickness of 20 Å, corresponding to 8 layers of the bulk oxide (compare with figure 2(b)), was needed to accurately detect the (004) PdO(101) peak. Since the (004) PdO(101) is moreover located on the specular (00*l*) rod of the sample, a certain out-of-plane mosaicity of the PdO crystallites is usually required in addition to fulfill the diffraction condition. In the present case, the thus created time-delay was estimated to 1 s only, and can accordingly be neglected. As the islands grow larger during the oxidation process, signals from the bulk oxide become finally also detectable by HESXRD. This scenario would explain the delayed HESXRD Bragg peak signal upon oxidation.

During the reduction, the PdO islands first transform into metallic islands. In the HESXRD this is immediately detected as the sudden decrease in intensities of the PdO Bragg peaks and their disappearance, since the interlayer distances changes to that of the metal. The surface, at this late oxidation stage, features an immense extent of surface roughness, in line with the notion of a Stransky-Krastanov growth and the XRR results. We assume, in line with conclusions reported earlier [21], that the SOR technique is more sensitive to changes in optical constants than to changes in surface morphology. However, in the specific case of such a highly roughened surface we suppose that the specularly reflected LED light is reduced to such a great extent that changes in the optical properties become indistinguishable for the SOR technique. Accordingly, SOR appears in this case to be more sensitive to changes in morphology and/or the roughness as compared to changes in the optical constant. Thus, the SOR signal changes more rapidly during the subsequent smoothening [10, 38] of the surface due to the elevated temperature, while the HESXRD is less sensitive to this process. This would explain the delayed SOR signal upon reduction. The proposed scenario for the reduction has support from previous investigations, as the formation of metallic islands and their subsequent smoothening in the transition to a reducing gas environment have also been evidenced in earlier operando STM studies during CO oxidation over Pd(100) [38].

In this context, it is important to emphasize that at the initial oxidation stage, changes in the SOR correlated to the appearance of a well-ordered 2D Pd surface oxide layer (corresponding to one layer of the bulk oxide shown in figure 2(b)). Thus, the data imply that SOR can detect the formation of a surface oxide layer which is only 2–3 Å thin (compare with interlayer distance of the PdO in figure 2(b)). Assuming a smooth, well-ordered surface oxide wetting the sample surface, the data presented in this report are in line with earlier findings indicating that SOR appears more sensitive to changes in the optical properties of the material as compared to changes in the surface roughness [21].

One approach to further improve the calibration and understanding of the sensitivity of SOR would be to study already atomic-scale well-characterized materials combinations such as surface reconstructions, surface oxides [39] and thin film oxide formation [40]. In such systems the change

in surface roughness is negligible, and only the change in the SOR signal due to the change in optical constant should be detected. In addition, to investigate the influence of the surface morphology on the SOR sensitivity while excluding any influence from changes in optical constants, in-situ SOR measurements could be carried out while sputtering the sample surface. Such approaches will require well-characterized surfaces under controlled conditions in UHV, combined with UHV surface techniques such as STM and LEED.

Apart from explaining the observations above, the present manuscript moreover demonstrates the potential use of SOR to detect a change in the surface morphology of planar model catalysts during surface oxidation under harsh conditions. It is clear that even a relatively small change of the surface can be detected as a change in the SOR signal, which makes the technique useful in many environments and experimental conditions. The temporal resolution is also high (up to 200 Hz), making it possible to detect oscillatory changes, such as in epitaxial growth by molecular beam epitaxy or atomic layer deposition. The technique can also be used in a liquid transparent to visible light such as water, opening the door for *in situ* experiments during electrochemical reactions at an electrode surface such as anodization or cyclic voltammetry or electrochemical atomic layer deposition. Further, the relatively low cost of the equipment for the SOR apparatus and the relative ease to assemble and to mount on various experimental equipment such as UHV chambers, reactors and electrochemical cells, makes it a low-cost and easy-to-use equipment to bring to for instance synchrotrons or other large scale facilities. Moreover, certain surface structures or morphologies may be studied under various conditions by SOR in a local lab before performing an experiment at large scale facilities. It is also clear that the spatial resolution, in the present report 100 μm, can easily be improved to around 1 μm resulting in a SOR microscope. With such resolution, grains and similar structures important for applied materials should be accessible, as have been shown by previous studies of pitting corrosion processes [18, 19].

5. Conclusions

In conclusion, we have acquired combined HESXRD and SOR data from a Pd(100) single crystal surface during *in situ* oxidation. Using HESXRD we followed the growth of the PdO bulk oxide with subsecond temporal resolution, where the final thickness was confirmed by XRR. The temporal differences between the SOR and HESXRD techniques in the detection of oxide formation and its reduction have been discussed, and the potential use of SOR in other applications has been proposed. Our conclusions are in line with previous findings indicating that SOR is more sensitive to changes in the optical constant of the surface than to changes in the surface roughness. The data moreover imply that SOR can detect the formation of an ultrathin PdO surface oxide layer of 2–3 Å thickness.

ORCID iDs

S Pfaff https://orcid.org/0000-0002-8528-9362
U Hejral https://orcid.org/0000-0002-4393-0983

References

[1] Somorjai G A and Li Y 2011 Impact of surface chemistry *Proc. Natl Acad. Sci.* **108** 917
[2] van Spronsenet M A, Frenken J W M and Groot I M N 2017 Surface science under reaction conditions: CO oxidation on Pt and Pd model catalysts *Chem. Soc. Rev.* **46** 4347
[3] Szanyi J and Goodman D W 1993 Combined elevated pressure reactor and ultrahigh vacuum surface analysis system *Rev. Sci. Instrum.* **64** 2350
[4] Ryczkowski J 2001 IR spectroscopy in catalysis *Catalysis Today* **68** 263
[5] Hartfelder U, Singh J, Haase J, Nachtegaal M, Grolimund D and van Bokhoven J A 2016 Detecting and utilizing minority phases in heterogeneous catalysis *Sci. Rep.* **6** 37597
[6] Shen Y R 1989 Surface properties probed by 2nd harmonic and sum frequency generation *Nature* **337** 519
[7] Salmeron M and Schlögel R 2008 Ambient Pressure Photoelectron Spectroscopy: A new tool for surface science and nanotechnology *Surf. Sci. Rep.* **63** 169
[8] Trotochaud L, Head A R, Karslioglu O, Kyhl L and Bluhm H 2017 Ambient pressure photoelectron spectroscopy: Practical considerations and experimental frontiers *J. Phys.: Condens. Matter* **29** 053002
[9] Toyoshima R, Kondoh H 2015 In-situ observations of catalytic surface reactions with soft x-rays under working conditions *J. Phys.: Condens. Matter* **27** 083003
[10] Frenken J W M and Groot I M N 2017 Live observations of catalysts using high-pressure scanning probe microscopy *Operando Research in Heterogeneous Catalysis* (Springer Series in Chemical Physics vol 114) (Cham: Springer) p 1
[11] Stierle A, Gustafson J and Lundgren E 2017 Surface-sensitive x-ray diffraction across the pressure gap *Operando Research in Heterogeneous Catalysis* (Springer Series in Chemical Physics vol 114) (Berlin: Springer) p 59
[12] Jinschek J R 2014 Advances in the environmental transmission electron microscope (ETEM) for nanoscale in situ studies of gas-solid interactions *Chem. Commun.* **50** 2696
[13] Over H 2012 Surface chemistry of ruthenium dioxide in heterogeneous catalysis and electrocatalysis: from fundamental to applied research *Chem. Rev.* **112** 3356
[14] Weaver J F 2013 Surface chemistry of late transition metal oxides *Chem. Rev.* **113** 4164
[15] Lundgren E *et al* 2015 The surface oxide as a source of O on Rh(111) *J. Electron Spectrosc. Relat. Phenom.* **144** 367
[16] Gustafson J *et al* 2018 The role of oxides in catalytic co oxidation over rhodium and palladium *ACS Catal.* **8** 4438

[17] Mehar V *et al* 2018 Understanding the intrinsic surface reactivity of single-layer and multilayer PdO (101) on Pd (100) *ACS Catal.* **8** 8553

[18] Punckt C, Bölscher M, Rotermund H H, Mikhailov A S, Organ L, Budiansky N, Scully J R and Hudson J L 2004 Sudden onset of pitting corrosion on stainless steel as a critical phenomenon *Science* **305** 1133

[19] Klages P E, Rotermund M K and Rotermund H H 2012 Simultaneous holographic, ellipsometric and optical imaging of pitting corrosion on SS 316LVM stainless steel *Corros. Sci.* **65** 128

[20] Onderwaater W G, Taranovskyy A, Bremmer C M, van Baarle G C, Frenken J W M and Groot I M N 2017 From dull to shiny: A novel setup for reflectance difference analysis under catalytic conditions *Rev. Sci. Instrum.* **88** 023704

[21] Onderwaater W G, Taranovskyy A, Bremmer C M, van Baarle G C, Frenken J W M and Groot I M N 2017 In Situ optical reflectance difference observations of CO oxidation over Pd(100) *J. Phys. Chem.* C **121** 11407

[22] Zhou J, Blomberg S, Gustafson J, Lundgren E and Zetterberg J 2017 Simultaneous imaging of a gas phase over and surface reflectance of a Pd(100) single crystal during CO oxidation *J. Phys. Chem.* C **121** 23511

[23] Pfaff S *et al* 2019 Combining HESXRD with SOR and PLIF for operando catalyst surface characterization *Rev. Sci. Instrum.* **90** 033703

[24] Schell N, King A, Beckmann F, Fischer T, Müller M and Schreyer A 2014 The high energy materials science beamline (HEMS) at PETRA III *Mater. Sci. Forum* **772** 57

[25] van Rijn R *et al* 2010 Ultrahigh vacuum/high-pressure flow reactor for surface x-ray diffraction and grazing incidence small angle x-ray scattering studies close to conditions for industrial catalysis *Rev. Sci. Instrum.* **81** 014101

[26] Blomberg S *et al* 2018 Combining synchrotron light with laser technology in catalysis research *J. Synchrotron Radiat.* **25** 1389

[27] Stierle A, Kasper N, Dosch H, Lundgren E, Gustafson J, Mikkelsen A and Andersen J N 2005 A surface x-ray study of the structure and morphology of the oxidized Pd(001) surface *J. Chem. Phys.* **122** 044706

[28] Abbin A, Hakanoglu C, Asthagiri and Weaver J F 2012 Dispersion-corrected density functional theory calculations of the molecular binding of n-alkanes on Pd(111) and PdO(101) *J. Chem. Phys.* **136** 054702

[29] Björck M and Andersson G 2007 GenX: an extensible x-ray reflectivity refinement program utilizing differential evolution *J. Appl. Cryst.* **40** 1174

[30] Gustafson J *et al* 2014 High-energy surface x-ray diffraction for fast surface structure determination *Science* **343** 758

[31] Shipilin M *et al* 2014 Quantitative surface structure determination using in situ high-energy SXRD: Surface oxide formation on Pd(100) during catalytic CO oxidation *Surf. Sci.* **630** 229

[32] Shipilin M *et al* 2015 Transient structures of PdO during CO Oxidation over Pd(100) *J. Phys. Chem.* C **119** 15469

[33] Shipilin M *et al* 2017 The influence of incommensurability on the long-range periodicity of the Pd(100)-$(\sqrt{5} \times \sqrt{5})R27°$ -PdO(101) *Surf. Sci.* **660** 1

[34] Fromhold A T Jr and Cook E L 1967 Kinetics of oxide film growth on metal crystals: thermal electron emission and ionic diffusion *Phys. Rev.* **163** 650

[35] Fromhold A T Jr and Cook E L 1966 Shottky emission as a rate-limiting factor in thermal oxidation of metals *Phys. Rev. Lett* **17** 1212

[36] Fromhold A T Jr and Cook E L 1966 Kinetics of oxide film growth on metal crystals: electron tunneling and ionic diffusion *Phys. Rev.* **158** 600

[37] Cabrera N and Mott N F 1949 Theory of the oxidation of metals *Rep. Prog. Phys.* **12** 163

[38] Hendriksen B L M, Bobaru S C and Frenken J W M 2004 Oscillatory CO oxidation on Pd(1 0 0) studied with in situ scanning tunneling microscopy *Surf. Sci.* **552** 229

[39] Lundgren E, Mikkelsen A, Andersen J N, Kresse G, Schmid M and Varga P 2006 Surface oxides on close-packed surfaces of late transition metals *J. Phys. Condens. Matter* **18** 481

[40] Merte L R, Shipilin M, Ataran S, Blomberg S, Zhang C, Mikkelsen A, Gustafson J and Lundgren E 2015 Growth of ultra-thin iron oxide films on Ag(100) *J. Chem. Phys.* C **119** 2572